Suppression of *Arabidopsis* protophloem differentiation and root meristem growth by CLE45 requires the receptor-like kinase BAM3

Stephen Depuydt[1], Antia Rodriguez-Villalon[1], Luca Santuari, Céline Wyser-Rmili, Laura Ragni, and Christian S. Hardtke[2]

Department of Plant Molecular Biology, University of Lausanne, CH-1015 Lausanne, Switzerland

Edited by Philip N. Benfey, Duke University, Durham, NC, and approved March 20, 2013 (received for review December 20, 2012)

Peptide signaling presumably occupies a central role in plant development, yet only few concrete examples of receptor-ligand pairs that act in the context of specific differentiation processes have been described. Here we report that second-site null mutations in the *Arabidopsis* leucine-rich repeat receptor-like kinase gene *barely any meristem 3* (*BAM3*) perfectly suppress the postembryonic root meristem growth defect and the associated perturbed protophloem development of the *brevis radix* (*brx*) mutant. The roots of *bam3* mutants specifically resist growth inhibition by the CLAVATA3/ENDOSPERM SURROUNDING REGION 45 (CLE45) peptide ligand. WT plants transformed with a construct for ectopic overexpression of CLE45 could not be recovered, with the exception of a single severely dwarfed and sterile plant that eventually died. By contrast, we obtained numerous transgenic *bam3* mutants transformed with the same construct. These transgenic plants displayed a WT phenotype, however, supporting the notion that CLE45 is the likely BAM3 ligand. The results correlate with the observation that external CLE45 application represses protophloem differentiation in WT, but not in *bam3* mutants. *BAM3*, *BRX*, and *CLE45* are expressed in a similar spatiotemporal trend along the developing protophloem, up to the end of the transition zone. Induction of *BAM3* expression upon CLE45 application, ectopic overexpression of *BAM3* in *brx* root meristems, and laser ablation experiments suggest that intertwined regulatory activity of *BRX*, *BAM3*, and *CLE45* could be involved in the proper transition of protophloem cells from proliferation to differentiation, thereby impinging on postembryonic growth capacity of the root meristem.

CLE peptides | vasculature

In plants, peptide signaling presumably occupies a central role because receptor and ligand genes are relatively abundant in their genomes (1–3). However, only a few examples of ligand-receptor pairs acting in specific developmental contexts have been described (4–7). The prototypical example is the leucine-rich repeat receptor-like kinase (LRR-RLK) CLAVATA 1 (CLV1), whose activity is modulated non–cell autonomously by its dodecapeptide ligand CLV3 to maintain stem cell niche homeostasis in the shoot meristem (8–10). Both CLV1 and CLV3 belong to larger clades of respective homologs, the CLV-like LRR-RLKs and the CLV3/ENDOSPERM SURROUNDING REGION (CLE) peptides. In *Arabidopsis*, the latter are represented by 31 genes, which sometimes encode the same processed dodecapeptide, thus giving rise to a family of 26 CLE peptides (11, 12). Interestingly, when applied at nanomolar concentrations, the majority of CLE peptides inhibit root growth, presumably by triggering terminal differentiation of stem cells and/or by suppressing protoxylem differentiation (11, 13). However, hardly any receptor–CLE ligand pairs with specific roles in root development have been identified, *Arabidopsis* CRINKLY 4 (ACR4)–CLE40 being the notable exception (4, 7). In this study, we show that the CLV-like LRR-RLK BARELY ANY MERISTEM 3 (BAM3) and its putative ligand CLE45 are involved in guiding progression of protophloem development in the *Arabidopsis* primary root meristem, which determines the meristem's postembryonic growth capacity. Our discovery emerged from a second-site suppressor screen of a null mutation in the *BREVIS RADIX* (*BRX*) gene. *BRX* encodes a putative transcriptional coregulator, which is subject to complex regulation at both the transcriptional and posttranslational level (14–18). In *brx* null mutants, postembryonic growth of the root meristem 3–6 d after germination (dag) is strongly decreased, leading to a smaller mature meristem and consequently slower root growth at later stages of development. This phenotype is associated with perturbed progression of protophloem development, which manifests in asynchronous differentiation of cells in the so-called protophloem transition zone (18) (see Fig. S1*A* for an overview of root meristem structure and terminology). This asynchronicity can be visualized by cell wall staining or marker gene expression and is accompanied by a shortened protophloem transition zone (18). Whether the perturbed progression of protophloem development in *brx* is a cause or a consequence of suspended postembryonic root meristem growth remains unclear.

Results and Discussion

To uncover genetic suppressors of the *brx* phenotypes, seeds homozygous for the T-DNA insertion null allele *brx-2* in the standard Col-0 WT background were mutagenized with ethyl methanesulfonate (EMS). Forty thousand progeny collected from 10,000 mutagenized plants were screened for rescue of the *brx-2* short root phenotype in tissue culture, and 33 mutants that significantly restored root growth to variable degrees were isolated (Fig. 1*A* and Fig. S1*B*). In this study, we investigated suppressor line 1.77.1, which displayed WT root growth vigor. Confocal microscopy at different stages revealed that meristem growth was indeed restored and that protophloem development appeared normal (Fig. 1 *B*–*D*). Likewise, root growth responses to hormone treatments, which are perturbed in *brx* (15, 18), resembled WT (Fig. 1*E*). To investigate whether this rescue was also associated with restoration of the extensive gene expression changes in *brx* mutants (15), we performed next generation sequencing (NGS) of mRNA isolated from the roots of 3-d-old seedlings (19). Analysis of these data using the "Tuxedo" pipeline (20) revealed numerous expression changes between *brx-2* and Col-0 as well as 1.77.1 seedlings, but also between 1.77.1 and Col-0 seedlings (Dataset S1). However, the expression of more than 86% of genes (i.e., 905 of 1,071 down-regulated genes, 619 of 685 up-regulated genes, or 1,524 out of 1,756 total

Author contributions: S.D., A.R.-V., and C.S.H. designed research; S.D., A.R.-V., C.W.-R., and L.R. performed research; S.D., A.R.-V., L.S., L.R., and C.S.H. analyzed data; and S.D., A.R.-V., and C.S.H. wrote the paper.

The authors declare no conflict of interest.

This article is a PNAS Direct Submission.

[1]S.D. and A.R.-V. contributed equally to this work.

[2]To whom correspondence should be addressed. E-mail: christian.hardtke@unil.ch.

This article contains supporting information online at www.pnas.org/lookup/suppl/doi:10.1073/pnas.1222314110/-/DCSupplemental.

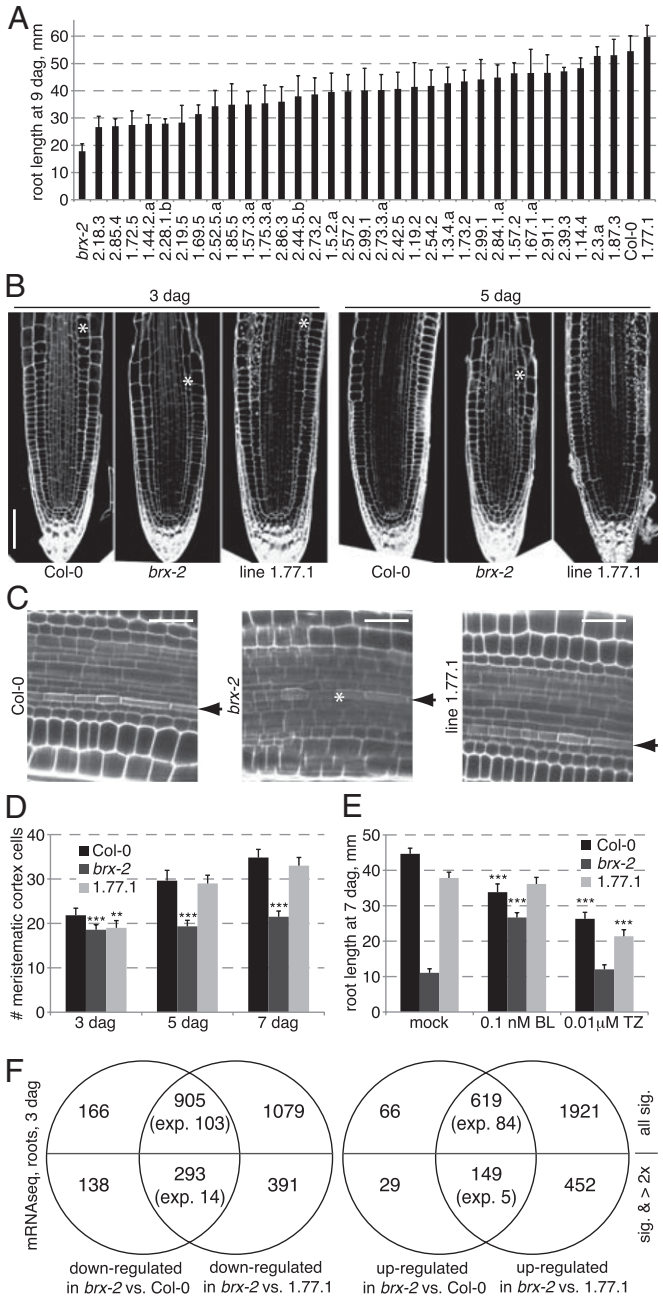

Fig. 1. Isolation of *brx* suppressors by second-site mutation screening. (*A*) Root length of suppressor lines at 9 dag. *brx-2* is a null allele in Col-0 WT background. All lines were significantly different ($P < 0.001$) from *brx-2*. (*B*) Root meristem growth between 3 and 5 dag visualized by mPS-PI staining. Asterisks indicate the first rapidly elongating cortex cell (out of range in Col-0 and line 1.77.1 at 5 dag). (*C*) Rescue of differentiation gaps in the protophloem transition zone of *brx-2* mutants (asterisk) in line 1.77.1 as revealed by mPS-PI staining. Arrowheads indicate protophloem cell files (enhanced PI staining). (*D*) Quantification of root meristem growth as expressed by meristematic cortex cell number. (*E*) Root growth response to brassinosteroid (brassinolide, BL) and cytokinin (transzeatin, TZ) application. (*F*) Overlaps of mRNA sequencing analysis of differential expression with different thresholds. (Scale bars: *B*, 100 μm; *C*, 50 μm.) Error bars represent SEM; $^{**}P < 0.01$; $^{***}P < 0.001$.

misexpressed genes) that were differentially expressed between *brx-2* and Col-0 was normalized in 1.77.1 (Fig. 1*F*), suggesting that the second-site mutation recovers the transcriptional program perturbed in *brx-2*. It is noteworthy that with respect to previously obtained microarray data (15), the overlap was significantly higher than expected by chance, but limited. This might in part reflect variation in developmental stage and individual growth conditions between experiments, but also that overall RNA sequencing detected fewer genes (i.e., with at least one read per gene in all samples) than microarray hybridization (i.e., signal above background). It is also worthwhile to point out that the set of differentially expressed genes determined by RNA sequencing very much depended on the bioinformatics pipeline applied to detect expression differences (e.g., ref. 21), although the transcriptome signature relations between samples stayed coherent over different analyses. Finally, we introduced a reporter gene of the only functional *BRX* homolog in *Arabidopsis*, *BRX-LIKE 1* (*BRXL1*) (22), into 1.77.1 to exclude that the rescue of *brx-2* phenotypes was due to ectopic *BRXL1* expression in the root meristem, which we could confirm (Fig. S1*C*).

To identify the causal mutation for the phenotypic reversion, we backcrossed the 1.77.1 line to its *brx-2* parent. In the progeny, the *brx-2* phenotype segregated at *ca.* 75%, confirming that the suppressor mutation is recessive. Thus, we prepared DNA from pools of *ca.* 50 short-root and long-root seedlings collected from this F2 generation and sequenced it by NGS (23). Mapping of the reads onto the *brx-2* reference genome sequenced in parallel revealed an interval on chromosome 4 in which the frequency of SNPs introduced by EMS mutagenesis increased sharply in the reads from the long root pool, with one particularly interesting nonsynonymous SNP reaching 100% frequency (Fig. S1*D*). Independent Sanger sequencing confirmed its exclusive homozygosity specifically in long-root individuals, suggesting that it caused the suppression of *brx-2* phenotypes. The SNP leads to a premature stop codon in the coding region of *BAM3*, thereby deleting the kinase domain of the protein and presumably leading to a loss of function (Fig. 2*A*). To confirm this notion, we obtained the null allele *bam3-2* (24) and crossed it to *brx-2*. The F2 segregation of short- and long-root individuals suggested that this allele also suppresses *brx-2* phenotypes, unlike a null mutation in the closest *BAM3* homolog, *BAM1* (Fig. 2*B*) (24). Finally, a similar approach to characterize the initially second best suppressor from our screen, line 1.87.3 (Fig. 1*A*), revealed a causal homozygous SNP that gives rise to an even earlier stop codon in *BAM3* (Fig. 2*A*). These independent examples suggest that *BAM3*

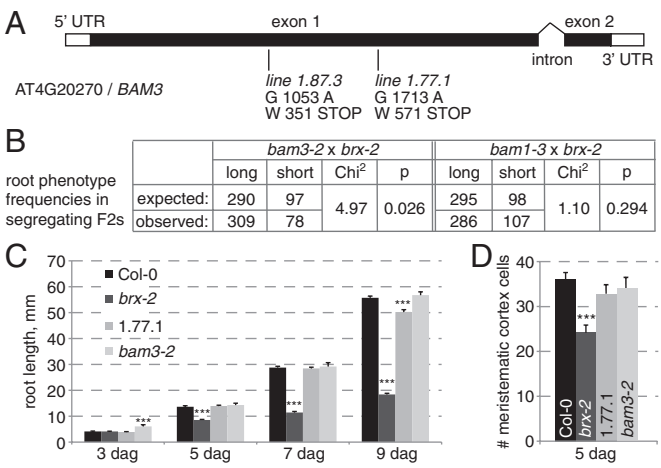

Fig. 2. Isolation and analysis of the *bam3* mutant as a *brx-2* suppressor. (*A*) Schematic presentation of the *BAM3* gene structure and the isolated suppressor mutations. (*B*) Segregation analysis of indicated crosses. *bam3-2* is a *BAM3* null allele; *bam1-3* is a null allele in its homolog *BAM1*. (*C*) Root growth progression and (*D*) mature root meristem size in indicated genotypes. Error bars represent SEM; Statistical significance in *C* and *D* is indicated in comparison with respective WT sample. $^{***}P < 0.001$.

loss of function rescues the root meristem growth and protophloem development defects of *brx-2* mutants. Interestingly, no apparent morphological phenotypes have been reported for the *bam3-2* single mutant (24), and root growth vigor is indeed normal in *bam3-2* (Fig. 2*C*), as is root meristem size (Fig. 2*D*).

To identify a putative BAM3 ligand, we next tested whether *bam3-2* mutants are resistant to treatment with any of the CLE peptides that have been reported to inhibit root growth (12, 25, 26). Indeed, in a tissue culture screen, *bam3-2* mutants displayed specific resistance to application of CLE45 peptide, which was the most powerful inhibitor of root growth (Fig. 3 *A–D*). Closer inspection by confocal microscopy revealed that CLE45 treatment inhibits root meristem growth in both Col-0 and *brx-2*, but hardly so in *bam3-2* (Fig. 3 *E* and *F*). The insensitivity of *bam3-2* to CLE45 activity was also supported by experiments that aimed to introduce a transgene for ectopic overexpression of *CLE45* under control of the *UBIQUITIN 10* promoter into WT and *bam3-2*. Whereas WT plants that carried this transgene could not be recovered with the exception of a single severely dwarfed and sterile plant that eventually died, numerous transgenic *bam3* mutants transformed with the same construct were obtained (Fig. S1*E*). The latter displayed a WT phenotype however, supporting the notion that CLE45 is the likely BAM3 ligand, although at this stage we cannot exclude the possibility that another RLK whose activity is *BAM3*-dependent is the CLE45 receptor. However, interestingly, neither mutant in the two closest *BAM3* homologs, *bam1* and *bam2*, displayed CLE45 resistance (Fig. 3*G*), suggesting that BAM3 and CLE45 constitute a highly specific putative receptor–ligand pair, matching their solitary outlier positions in their respective phylogenies (24, 25, 27). A survey of the suppressor lines indicated that, as expected, 1.77.1 and 1.87.3 are CLE45-resistant, whereas other lines, with two mildly resistant exceptions, are not (Fig. 3*H*). Although our data suggest that CLE45 needs BAM3 to act, our data do not exclude that other peptide ligands for BAM3 might exist, similar to the promiscuity described for BAM1 and BAM2 (28). It therefore appears possible that CLE45–BAM3 action is specifically relevant in the root meristem.

Further investigation of CLE45-treated roots revealed no apparent effects on stem cell niche morphology or quiescent center (QC) markers (Fig. 4*A*). By contrast, CLE45 application abolished the typically strong propidium iodide (PI) cell wall staining of protophloem cells (18), to the extent that no protophloem could be distinguished any longer (Fig. 4*B*). Consistent with this finding, CLE45 application excluded expression of the protophloem development marker *ALTERED PHLOEM DEVELOPMENT* (*APL*), which encodes a transcription factor that is required for phloem identity (29), from the meristematic zone (Fig. 4*C*). By contrast, no effect was observed on the protoxylem development marker *ARABIDOPSIS HISTIDINE-CONTAINING PHOSPHOTRANSFER PROTEIN 6* (*AHP6*) (30), other than adjustment of its zoning to the reduced meristem size (Fig. 4*D*). These results correlate with reduced and discontinuous expression of *APL* in *brx* mutants (18) (Fig. S1*F*). In summary, CLE45 treatment specifically affected root meristem growth and protophloem development, in striking similarity to *brx* loss of function. The negative effect of CLE45 on protophloem development is unique, because so far CLE peptides have been reported to rather interfere with protoxylem differentiation (11, 13).

Mimic of the *brx* phenotype by CLE45 application and its suppression by *bam3* loss of function suggested that the putative CLE45–BAM3 receptor–ligand pair might be hyperactive in *brx* mutants. To test this notion, we first surveyed transcriptomic effects of CLE45 application on 3-d-old seedling roots by NGS. This experiment yielded a set of differentially expressed genes (Dataset S2), of which more than 60% were also accordingly misregulated in *brx-2* (Fig. 4*E*). Thus, the aberrant transcriptome signature of *brx-2* mutants comprises the majority of CLE45-responsive genes. To check for transcriptional deregulation of

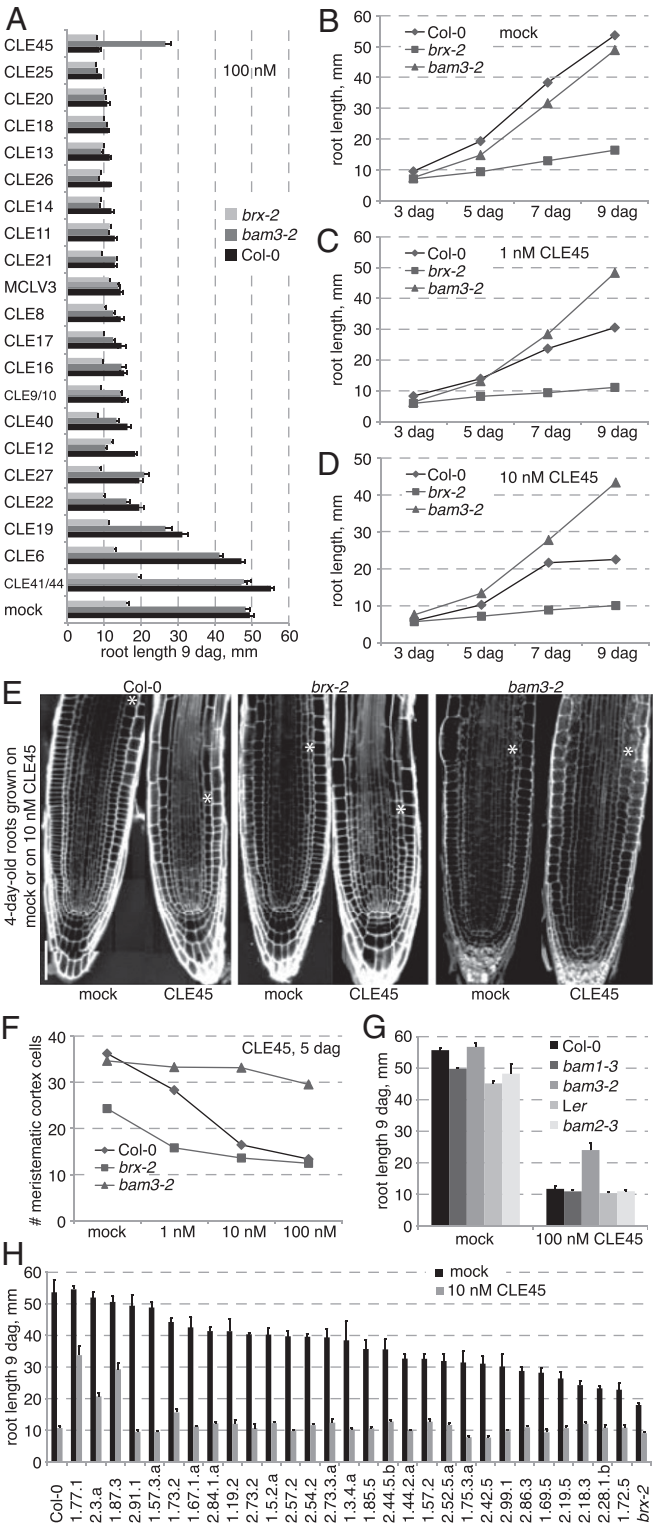

Fig. 3. Identification of the putative *BAM3* ligand. (*A*) Root growth of different genotypes on media containing indicated CLE peptide. (*B–D*) Dose–response of different genotypes to increasing amounts of CLE45 in the medium. (*E* and *F*) Effect of CLE45 application on root meristem growth. (*G*) Specific CLE45 resistance of *bam3*, but not of mutants in its homologs *bam1* and *bam2* (note that *bam2-3* is a *BAM2* null mutant in Landsberg *erecta* [Ler] background). (*H*) CLE45 resistance in the suppressor lines. (Scale bar: *E*, 100 μm.) Error bars represent SEM.

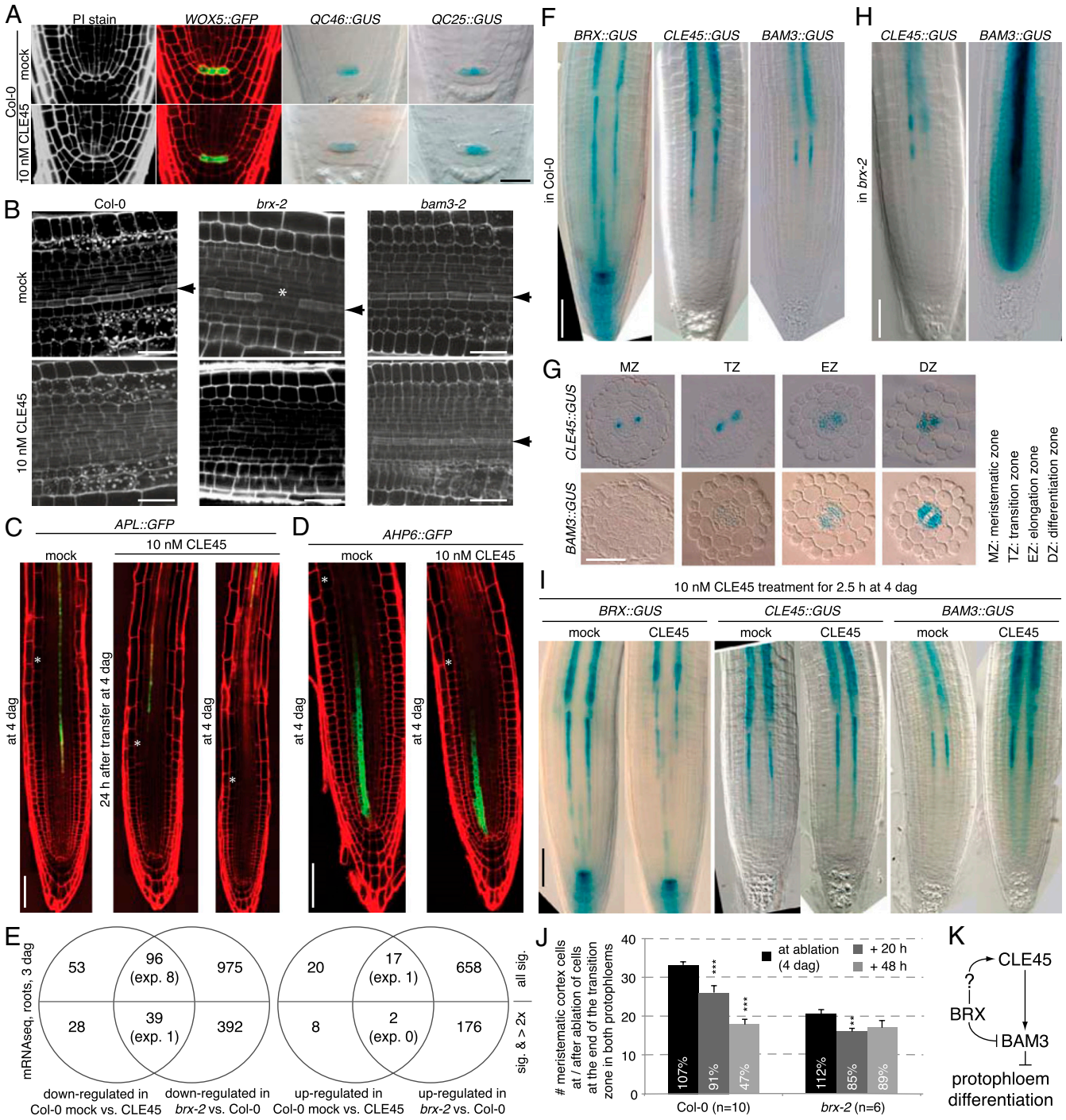

Fig. 4. CLE45 effect on protophloem differentiation and expression pattern analyses. (*A*) No alteration of stem cell niche morphology and QC marker expression upon growth on medium containing CLE45. (*B*) Inhibition of protophloem differentiation in the protophloem transition zone by CLE45 treatment as revealed by mPS-PI staining. Arrowheads indicate protophloem cell file (enhanced PI staining). (*C*) Exclusion of the expression of the protophloem development marker *APL* from the meristematic zone upon CLE45 treatment; (*D*) no effect on the protoxylem marker, *AHP6*. (*E*) Overlaps of CLE45-responsive genes determined by mRNA sequencing with differentially expressed genes between Col-0 and *brx-2* (Fig. 1*E*) for different thresholds. (*F* and *G*) Expression patterns of indicated reporter genes at 4 dag in the WT and (*H*) *brx-2* mutants. (*I*) Response of indicated reporter genes to CLE45 application. (*J*) Root meristem size shrinkage in Col-0 and *brx-2* after ablation of single cells in the transition zone of both protophloem strands. The relative size compared with the parallel nonablated control group is indicated in %. (*K*) Schematic of the regulatory relation between BRX, CLE45, and BAM3. (Scale bar: *A* and *B*, 50 μm; *C*, *D*, and *F*–*I*, 100 μm.) Error bars represent SEM; $^{**}P < 0.01$; $^{***}P < 0.001$.

CLE45 and *BAM3* in *brx-2*, we investigated their expression by reporter gene assays. In WT, this revealed a strikingly precise overlap of the expression patterns of all three genes (Fig. 4*F*). Similar to *BRX*, both *CLE45* and *BAM3* display gradually increasing expression along the developing protophloem, up to the end of its transition zone, after which expression switches to the pericycle. A spatiotemporal hierarchy of expression was apparent and also suggested by analysis of transverse root sections

along the meristem (Fig. 4*G*). Although *BRX* expression was already evident in the early meristematic zone, *CLE45* expression was only detected from the later meristematic zone onwards, whereas *BAM3* expression was not observed before the transition zone. In *brx-2* background, *CLE45* expression appeared to be slightly decreased and interrupted, reminiscent of *BRX* expression in *brx* mutants and correlating with the PI staining and *APL* expression gaps in the developing protophloem that are typical for *brx* mutants (16, 18). By contrast, the *BAM3* reporter displayed deregulated and ectopic transcription specifically in *brx-2* meristems, including extension of its expression domain into the entire stele and meristematic zone, down to the stem cell niche (Fig. 4*H*). This up-regulation was in tendency also detectable by quantitative PCR (qPCR) on mRNA prepared from whole roots (Fig. S1*G*). Finally, complementing these results, CLE45 treatment resulted in up-regulation of *BAM3* expression (Fig. 4*I* and Fig. S1*G*). Notably, the described expression changes were specific to the meristem and were not observed in the differentiated, mature parts of the root.

The formal interpretation of our data posits that *BRX* antagonizes *BAM3* activity, likely by restricting its expression level and domain, which, however, does not necessarily imply direct regulation. Although we found no evidence for transcriptional hyperactivity of *CLE45* in *brx*, it is conceivable that posttranslational CLE45 regulation could be directly or indirectly *BRX*-dependent. Alternatively, the correlation of *CLE45* expression with the differentiation state in *brx* could mean that increasing *CLE45* expression is an intrinsic feature of protophloem development in WT. Subsequent CLE45-dependent up-regulation of *BAM3* might then serve as a break on the progression of protophloem development to guide its differentiation and assure its integrity. Thus, transcriptional *BAM3* hyperactivity in *brx* background could lead to stochastic, premature disruption of the differentiation program depending on local CLE45 levels, giving rise to the *brx* protophloem discontinuity. This interpretation is also consistent with our finding that CLE45 treatment still leads to aggravation of the *brx* phenotype.

From our data, we also could not decide whether it is the removal of ectopic *BAM3* or the removal of *BAM3* from the protophloem that is responsible for suppression of the *brx* phenotype. Thus, we sought to independently test whether continuous protophloem development is required to maintain root meristem growth. To this end, we targeted single protophloem cells at the end of the transition zone for laser ablation using a 2-photon microscope. Indeed, ablation of one cell in both protophloem strands led to a dramatic reduction in meristem size (Fig. 4*J*). In *brx-2* mutants, presumably because of the already impaired meristem growth, this effect was considerably weaker and only transiently significant. It is possible that the meristem shrinkage upon protophloem cell ablation is due to an interruption of nutrient flow from the cotyledons to the root meristem through the protophloem. However, considering that these seedlings are small and at a very early stage and were grown on media containing sucrose, nutrients could be simply taken up by diffusion. Alternatively, interruption of auxin flow through the protophloem might cause the meristem shrinkage and correlates with reduced auxin transport in *brx* meristems (18). Regardless, our experiment demonstrates that a continuous protophloem is needed for growth and maintenance of the root meristem, which could thus constitute the causal phenotype not only in *brx*, but also in other mutants, notably *octopus* (31).

In summary, the sensitized *brx-2* mutant background allowed us to discover a potential role of the leucine-rich repeat receptor-like kinase BAM3 in protophloem development. This notion is underscored by our finding that the peptide ligand CLE45 requires BAM3 to exert its negative effect on protophloem differentiation. Thus, *BRX*, *BAM3*, and *CLE45* might interact directly or indirectly (Fig. 4*K*) to guide the proper transition of protophloem cells from proliferation to differentiation, which in turn could determine postembryonic growth capacity of the root meristem. With the data reported in this study, we have defined the genetic frame to investigate this idea in more detail in the future.

Materials and Methods

Plant tissue culture, plant transformation, and molecular biology experiments, such as genomic DNA isolation, genotyping, qPCR, or sequencing were performed according to standard procedures as described previously (18).

Plant Materials. The *Arabidopsis* Columbia-0 (Col-0) and Landsberg *erecta* (Ler) WT lines, the null mutants *brx-2*, *bam1-3*, *bam2-3*, and *bam3-2*, and the transgenic reporter lines *BRX::β-glucuronidase* (*GUS*), *BRXL1::GUS*, *WUSCHEL-RELATED HOMEOBOX 5* (*WOX5*)*::GFP*, *QC25::GUS*, *QC46::GUS*, *APL::GFP*, and *AHP6::GFP* have been described previously (17, 18, 24, 29, 30, 32).

EMS Mutagenesis. For EMS mutagenesis, 40.000 *brx-2* seeds were treated with a PBS containing 1.6% wt/vol EMS as described (33). After treatment, seeds were stratified at 4 °C for 3 d and then immediately planted on soil. Seeds from surviving plants were harvested in pools of five plants, giving rise to 2,000 pools. This M2 generation was immediately screened in tissue culture on standard half-strength Murashige and Skoog medium (pH 5.7) supplemented with 1% (wt/vol) sucrose. Per pool, 200 plants were screened and only plants with a clearly longer root than the control *brx-2* line at 9 dag were transferred onto soil. After confirmation of *brx-2* homozygosity and selfing, the 209 putative suppressor mutants were rescreened in the M3 generation to yield a final collection of 33 mutants.

CLE Peptide Treatments. CLE peptides (unmodified) were obtained by custom synthesis with >75% purity (Genscript) and dissolved in nanopure sterile water to give 1 mM stock solutions. For treatments, CLE peptides were diluted in autoclaved solid or liquid tissue culture media.

BAM3 and CLE45 Reporter Gene Construction. To obtain the *CLE45::GUS* construct, a 2 kb of genomic DNA upstream of the initiation codon was amplified by PCR using the oligonucleotides 5′-CAA CAA CAT TCA AGA TTT CAC-3′ and 5′-TTC TGC TCT TAG GCA GAC AAG-3′. The promoter fragments were then introduced into binary vector pMDC-162 to drive the expression of the GUS reporter. To generate the *BAM3::GUS* construct, the 2.2-kb *BAM3* 5′ upstream region was amplified by PCR using oligonucleotides 5′-GAT CAC ATA CCA CAT TGA TCT GC-3′ and 5′-GCT CAC TAT GTT CTG GAG TT-3′ and cloned as a KpnI–NcoI fragment into the binary vector pCAMBIA 1305.1. All binary constructs were introduced into *Arabidopsis* lines by *Agrobacterium*-mediated transformation following standard procedures (18).

Microscopy. For visualization by confocal (Zeiss LSM 510 Meta) or 2-photon (Zeiss LSM 710 NLO with a Ti:Sapphire Chameleon Ultra II infrared laser for acquisition) microscopy, roots were either stained by the modified pseudo-Schiff (mPS)-PI method or by PI only (18, 34). Both methods highlight the developing protophloem, which is stained stronger than the surrounding tissues (18, 34). GUS staining and light microscopy were performed according to standard procedures using a compound microscope. All images shown within one experiment were taken with identical settings. For GUS reporter line cross-sections, roots were embedded in plastic resin, sectioned, and visualized as previously described (18). Protophloem ablation experiments were performed with a 2-photon microscope. Briefly, roots were stained with 10 μg/mL PI on slides to visualize cellular structure and target the first transition zone cells in both protophloem strands for laser ablation. After ablation, seedlings were washed and put back into tissue culture to be grown on vertical plates. Meristem size was determined at different time points by repeatedly subjecting the same roots to confocal microscopy after PI staining, washing, and return onto tissue culture medium. Control seedlings were handled in exactly the same way in parallel, except that no laser ablation was performed.

Whole Genome Sequencing and Data Analysis. For mapping of the causal suppressor mutations, genomic DNA was prepared according to standard procedures from root tissue of bulked short-root or long-root segregants in the F2 from a back cross of the suppressor mutants to the *brx-2* parent line. To minimize plastid DNA contamination, root cultures were set up by pooling plants and growing them in liquid medium supplemented with 3% sucrose for 7 d under continuous light conditions. The DNA from the *brx-2* parental line and the short- and long-root pools were then sequenced to obtain 76-bp paired-end reads with standard insert size distribution. The

sequencing was performed at the Lausanne Genomics Technologies Facility at the University of Lausanne, using an Illumina HiSEq. 2000 sequencing machine, with one sample for each lane of the Illumina "flow cell." Reads were mapped on the TAIR10 *Arabidopsis* genome sequence using the read mapping tool bwa (version 0.5.9-r16) (35), and read alignment files in the .bam file format were generated with samtools (version 0.1.18-dev) (36). The bam alignment files were used to call SNPs using the UnifiedGenotyper SNP caller (37) from the Genome Analysis Toolkit (GATK) (38). With the intersectBed command of BEDTools (version 2.14.2) (39) on the variant calling format SNP files that were generated by the GATK, SNPs with more than 80% frequency in the *brx-2* parental line were considered as background SNPs and filtered out from the SNP list of the mutant pools. Only EMS-induced SNPs segregating with a frequency of more than 80% in the DNA from the long-root pools and with a frequency of less than 50% in the short-root pools were considered, with the thresholds accounting for variability from the sequencing and the read mapping steps. The SNPEff tool (40) was used to analyze the effect of the EMS-induced SNPs on gene coding sequences.

RNA Sequencing. For RNA sequencing, 3-d-old roots of the different genotypes were harvested and frozen in liquid nitrogen before total RNA was prepared using a QIAGEN RNeasy Plant Kit. For CLE45 treatment, WT seedlings were grown on meshes and at 3 dag were transferred to float on liquid mock medium or medium containing 10 nM CLE45 for 3 h before roots were harvested. cDNA synthesis, amplification, size selection, and high-throughput sequencing was carried out as described (19), except that cDNA synthesis was primed by poly-T-oligonucleotides. Differential expression was determined by analyzing the data through the "Tuxedo" pipeline (20).

qPCR Oligonucleotides. For gene expression quantification by qPCR, the following oligonucleotides were used: 5′-CAT TCA AAT CAA GCA AGA GAC G-3′ and 5′-GGC TGA GCT TTG TTG TGG AT-3′ for *CLE45*; 5′-CGT CGT TTT AGC TGT GGT CA-3′ and 5′-TGC AAC TTC TTC TCC GTT TG-3′ for *BAM3*; and 5′-GGT CAC CAA GGC TGC AGT GAA GAA-3′ and 5′-GCT CAA ACG CCA TCA AAG TTT TAA GAA-3′ for *ELONGATION FACTOR 1*.

ACKNOWLEDGMENTS. We thank Dr. E. Scacchi for comments on the manuscript. This work was funded by Swiss National Science Foundation Grant 31003A_129783 (to C.S.H.), a Marie-Curie postdoctoral fellowship (to S.D.), and European Molecular Biology Organization postdoctoral fellowships (to A.R.-V. and L.R.).

1. Butenko MA, Vie AK, Brembu T, Aalen RB, Bones AM (2009) Plant peptides in signalling: Looking for new partners. *Trends Plant Sci* 14(5):255–263.
2. Katsir L, Davies KA, Bergmann DC, Laux T (2011) Peptide signaling in plant development. *Curr Biol* 21(9):R356–R364.
3. De Smet I, Voss U, Jürgens G, Beeckman T (2009) Receptor-like kinases shape the plant. *Nat Cell Biol* 11(10):1166–1173.
4. De Smet I, et al. (2008) Receptor-like kinase ACR4 restricts formative cell divisions in the Arabidopsis root. *Science* 322(5901):594–597.
5. Etchells JP, Turner SR (2010) The PXY-CLE41 receptor ligand pair defines a multifunctional pathway that controls the rate and orientation of vascular cell division. *Development* 137(5):767–774.
6. Hirakawa Y, et al. (2008) Non-cell-autonomous control of vascular stem cell fate by a CLE peptide/receptor system. *Proc Natl Acad Sci USA* 105(39):15208–15213.
7. Stahl Y, Wink RH, Ingram GC, Simon R (2009) A signaling module controlling the stem cell niche in Arabidopsis root meristems. *Curr Biol* 19(11):909–914.
8. Clark SE, Williams RW, Meyerowitz EM (1997) The CLAVATA1 gene encodes a putative receptor kinase that controls shoot and floral meristem size in Arabidopsis. *Cell* 89(4):575–585.
9. Kondo T, et al. (2006) A plant peptide encoded by CLV3 identified by in situ MALDI-TOF MS analysis. *Science* 313(5788):845–848.
10. Ogawa M, Shinohara H, Sakagami Y, Matsubayashi Y (2008) Arabidopsis CLV3 peptide directly binds CLV1 ectodomain. *Science* 319(5861):294.
11. Ito Y, et al. (2006) Dodeca-CLE peptides as suppressors of plant stem cell differentiation. *Science* 313(5788):842–845.
12. Kinoshita A, et al. (2007) Gain-of-function phenotypes of chemically synthetic CLAVATA3/ESR-related (CLE) peptides in Arabidopsis thaliana and Oryza sativa. *Plant Cell Physiol* 48(12):1821–1825.
13. Jun J, et al. (2010) Comprehensive analysis of CLE polypeptide signaling gene expression and overexpression activity in Arabidopsis. *Plant Physiol* 154(4):1721–1736.
14. Mouchel CF, Briggs GC, Hardtke CS (2004) Natural genetic variation in Arabidopsis identifies BREVIS RADIX, a novel regulator of cell proliferation and elongation in the root. *Genes Dev* 18(6):700–714.
15. Mouchel CF, Osmont KS, Hardtke CS (2006) BRX mediates feedback between brassinosteroid levels and auxin signalling in root growth. *Nature* 443(7110):458–461.
16. Santuari L, et al. (2011) Positional information by differential endocytosis splits auxin response to drive Arabidopsis root meristem growth. *Curr Biol* 21(22):1918–1923.
17. Scacchi E, et al. (2009) Dynamic, auxin-responsive plasma membrane-to-nucleus movement of Arabidopsis BRX. *Development* 136(12):2059–2067.
18. Scacchi E, et al. (2010) Spatio-temporal sequence of cross-regulatory events in root meristem growth. *Proc Natl Acad Sci USA* 107(52):22734–22739.
19. Dorcey E, et al. (2012) Context-dependent dual role of SKI8 homologs in mRNA synthesis and turnover. *PLoS Genet* 8(4):e1002652.
20. Trapnell C, et al. (2012) Differential gene and transcript expression analysis of RNA-seq experiments with TopHat and Cufflinks. *Nat Protoc* 7(3):562–578.
21. Anders S, Huber W (2010) Differential expression analysis for sequence count data. *Genome Biol* 11(10):R106.
22. Briggs GC, Mouchel CF, Hardtke CS (2006) Characterization of the plant-specific BREVIS RADIX gene family reveals limited genetic redundancy despite high sequence conservation. *Plant Physiol* 140(4):1306–1316.
23. Santuari L, et al. (2010) Substantial deletion overlap among divergent Arabidopsis genomes revealed by intersection of short reads and tiling arrays. *Genome Biol* 11(1):R4.
24. DeYoung BJ, et al. (2006) The CLAVATA1-related BAM1, BAM2 and BAM3 receptor kinase-like proteins are required for meristem function in Arabidopsis. *Plant J* 45(1):1–16.
25. Kondo Y, Hirakawa Y, Kieber JJ, Fukuda H (2011) CLE peptides can negatively regulate protoxylem vessel formation via cytokinin signaling. *Plant Cell Physiol* 52(1):37–48.
26. Whitford R, Fernandez A, De Groodt R, Ortega E, Hilson P (2008) Plant CLE peptides from two distinct functional classes synergistically induce division of vascular cells. *Proc Natl Acad Sci USA* 105(47):18625–18630.
27. Sawa S, Kinoshita A, Nakanomyo I, Fukuda H (2006) CLV3/ESR-related (CLE) peptides as intercellular signaling molecules in plants. *Chem Rec* 6(6):303–310.
28. Guo Y, Han L, Hymes M, Denver R, Clark SE (2010) CLAVATA2 forms a distinct CLE-binding receptor complex regulating Arabidopsis stem cell specification. *Plant J* 63(6):889–900.
29. Bonke M, Thitamadee S, Mähönen AP, Hauser MT, Helariutta Y (2003) APL regulates vascular tissue identity in Arabidopsis. *Nature* 426(6963):181–186.
30. Mähönen AP, et al. (2006) Cytokinin signaling and its inhibitor AHP6 regulate cell fate during vascular development. *Science* 311(5757):94–98.
31. Truernit E, Bauby H, Belcram K, Barthélémy J, Palauqui JC (2012) OCTOPUS, a polarly localised membrane-associated protein, regulates phloem differentiation entry in Arabidopsis thaliana. *Development* 139(7):1306–1315.
32. Blilou I, et al. (2005) The PIN auxin efflux facilitator network controls growth and patterning in Arabidopsis roots. *Nature* 433(7021):39–44.
33. Weigel D, Glazebrook J (2002) *Arabidopsis, A Laboratory Manual* (Cold Spring Harbor Lab Press, Woodbury, NY).
34. Truernit E, et al. (2008) High-resolution whole-mount imaging of three-dimensional tissue organization and gene expression enables the study of Phloem development and structure in Arabidopsis. *Plant Cell* 20(6):1494–1503.
35. Li H, Durbin R (2009) Fast and accurate short read alignment with Burrows-Wheeler transform. *Bioinformatics* 25(14):1754–1760.
36. Li H, et al.; 1000 Genome Project Data Processing Subgroup (2009) The Sequence Alignment/Map format and SAMtools. *Bioinformatics* 25(16):2078–2079.
37. DePristo MA, et al. (2011) A framework for variation discovery and genotyping using next-generation DNA sequencing data. *Nat Genet* 43(5):491–498.
38. McKenna A, et al. (2010) The Genome Analysis Toolkit: a MapReduce framework for analyzing next-generation DNA sequencing data. *Genome Res* 20(9):1297–1303.
39. Quinlan AR, Hall IM (2010) BEDTools: A flexible suite of utilities for comparing genomic features. *Bioinformatics* 26(6):841–842.
40. Cingolani P, et al. (2012) A program for annotating and predicting the effects of single nucleotide polymorphisms, SnpEff: SNPs in the genome of Drosophila melanogaster strain w1118; iso-2; iso-3. *Fly (Austin)* 6(2):80–92.